HHS Public Access

Author manuscript

Anal Chem. Author manuscript; available in PMC 2021 December 09.

Published in final edited form as:

Anal Chem. 2021 October 12; 93(40): 13658–13666. doi:10.1021/acs.analchem.1c03085.

Smartphone-Based Dual-Channel Immunochromatographic Test Strip with Polymer Quantum Dot Labels for Simultaneous Detection of Cypermethrin and 3-Phenoxybenzoic Acid

Yuting Zhao[‖],
School of Mechanical and Materials Engineering, Washington State University, Pullman, Washington 99164, United States

Xiaofan Ruan[‖],
School of Mechanical and Materials Engineering, Washington State University, Pullman, Washington 99164, United States

Yang Song[‖],
School of Mechanical and Materials Engineering, Washington State University, Pullman, Washington 99164, United States;

Jordan N. Smith,
Exposure Science and Pathogen Biology, Pacific Northwest National Laboratory, Richland, Washington 99352, United States;

Natalia Vasylieva,
Department of Entomology and Nematology and UCD Comprehensive Cancer Center, University of California, Davis, Davis, California 95616, United States

Bruce D. Hammock,
Department of Entomology and Nematology and UCD Comprehensive Cancer Center, University of California, Davis, Davis, California 95616, United States;

Yuehe Lin,
School of Mechanical and Materials Engineering, Washington State University, Pullman, Washington 99164, United States;

Dan Du
School of Mechanical and Materials Engineering, Washington State University, Pullman, Washington 99164, United States;

Corresponding Authors: Yuehe Lin – School of Mechanical and Materials Engineering, Washington State University, Pullman, Washington 99164, United States; yuehe.lin@wsu.edu, **Dan Du** – School of Mechanical and Materials Engineering, Washington State University, Pullman, Washington 99164, United States; annie.du@wsu.edu.

[‖]Y.Z., X.R., and Y.S. contributed equally to this work.

Supporting Information

The Supporting Information is available free of charge at https://pubs.acs.org/doi/10.1021/acs.analchem.1c03085.

Structure of hapten; schematic side view showing the inner structure of the 3D-printed device; TEM image, HRTEM image, Raman spectrum, XPS spectrum, and XRD pattern of carbon dots; zeta potential of PCDs, PCDs-anti-pyrethroid Ab, and PCDs-anti-3-PBA Ab; optimization of experimental parameters for the dual-channel ICTS; and photograph of different fluorescence intensities in the proposed ITS assay for 3-PBA and cypermethrin (PDF)

Complete contact information is available at: https://pubs.acs.org/10.1021/acs.analchem.1c03085

The authors declare no competing financial interest.

Abstract

Currently, gas chromatography–mass spectrometry (GC–MS) and liquid chromatography–MS (LC–MS) are the primary methods used to detect pesticides and their metabolites for biomonitoring of exposure. Although GC–MS and LC–MS can provide accurate and sensitive measurements, these techniques are not suitable for point-of-care or in-field biomonitoring applications. The objective of this work is to develop a smartphone-based dual-channel immunochromatographic test strip (ICTS) for on-site biomonitoring of exposure to cypermethrin by simultaneous detection of cypermethrin and its metabolite, 3-phenoxybenzoic acid (3-PBA). Polymer carbon dots (PCDs) with ultrahigh fluorescent brightness were synthesized and used as a signal amplifier in ICTS assay. Cypermethrin (a representative pyrethroid pesticide) and its major metabolite 3-PBA were simultaneously detected to provide more comprehensive analysis of cypermethrin exposure. After competitive immunoreactions between the target sample and the coating antigens preloaded on the test line, the tracer antibody (PCD-conjugated antibody) was quantitatively captured on the test lines. The captured PCDs were inversely proportional to the amount of the target compound in the sample. The red fluorescence on the test line was then recorded using a smartphone-based device capable of conducting image analysis and recording. Under optimal conditions, the sensor showed excellent linear responses for detecting cypermethrin and 3-PBA ranging from 1 to 100 ng/mL and from 0.1 to 100 ng/mL, respectively, and the limits of detection were calculated to be ~0.35 ng/mL for cypermethrin and ~0.04 ng/mL for 3-PBA. The results demonstrate that the ICTS device is promising for accurate point-of-care biomonitoring of pesticide exposure.

Graphical Abstract

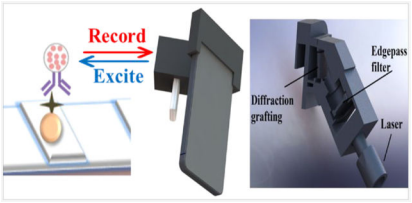

Pyrethroids are a class of compounds derived from natural pyrethrins used as pesticides to control pests and disease vectors in agricultural and residential use. The use of pyrethroids has increased over the last 20 years because pyrethroids have been replacing organophosphorus insecticides as relatively safer alternatives for pest control.[1,2] Pyrethroids interfere with voltage-sensitive sodium channels by slowing rates of ion-channel activation/deactivation, shifting the membrane potential to a hyperpolarized state as a primary mechanism of action.[3] Insects are more vulnerable to toxic effects of pyrethroids compared to mammals; however, toxicity may be realized in humans following high exposures.[3] Humans are primarily exposed to pyrethroids through diet, although drinking water, air, or dust may also serve as exposure routes.[4] Upon ingestion, most pyrethroids are rapidly hydrolyzed by carboxylesterases. Hydrolyzation of many pyrethroids including cypermethrin, permethrin, esfenvalerate, and deltamethrin releases 3-phenoxybenzoic acid (3-PBA) as a common nonspecific metabolite.[5,6] As such, many researchers, including those in the U.S. National Health and Nutrition Examination Survey (NHANES), and

the Canadian Health Measures Survey (CHMS) utilize 3-PBA as a urinary biomarker for pyrethroid exposure.[7,8]

Conventional liquid chromatography with mass spectrometry (LC–MS),[9,10] gas chromatography with MS techniques,[11,12] and the emerging immunoassays are the widely acceptable methods to detect pesticide exposure.[13,14] Although these techniques can provide accurate and sensitive results, complicated procedures and expensive laboratory equipment limit their ability to provide on-site measurements in clinical or field settings. Over the past decades, the Hammock group has developed novel strategies utilizing immunoassays to measure pyrethroid exposure.[15–23] While these assays have excellent sensitivity and throughput, they require laboratory-based instruments and skilled staff to obtain results, limiting their suitability for field and clinic screening. In recent years, immunochromatographic test strips (ICTSs) have been developed for pesticide detection.[24–28] For example, we have developed a Pt–Pd nanoparticle-based platform for simultaneous detection of dual biomarkers from exposure to organophosphorus pesticides.[29] The one-step, automated separation makes this assay simple, rapid, and user-friendly in various environments. Additionally, the inexpensive cost, the ability to be miniaturized, and easily visualized outputs make ICTSs ideal for field or clinical measurements.[30,31] Colloidal gold nanoparticles have been integrated with commercialized ICTSs as colorimetric probes for enhanced stability (e.g., human chorionic gonadotropin and human immunodeficiency virus test strips).[32,33] However, the low sensitivity remains a major challenge for more widespread application of this strategy.

New nanomaterials with fluorescent properties are being applied to construct ICTSs to improve the sensitivity.[34,35] Among the fluorescent labels, inorganic quantum dots (QDs) appear to be more attractive than fluorescent dyes and proteins because of their high quantum yields, narrow-band emissions, and resistance to photobleaching. For example, Zou et al. integrate a QD-based fluorescence ICTS assay with a test strip reader to develop a sensitive immunosensor for detection of 3,5,6-trichloropyridinol (limit of detection ~1.0 ng/mL), a primary metabolite of chlorpyrifos.[36] Nonetheless, common QD fluorescence can be easily quenched by metal nanoparticles, small molecules, or even themselves, so methods to improve photostability are necessary. Converting QDs into polymer dots may provide a viable strategy to improve photostability. In comparison with QDs, polymer dots offer increased fluorescence brightness and stability, which can improve detection sensitivity and decrease background interference of physiological matrixes. Fang et al. developed polymer dot-based ICTSs for simultaneously screening three kinds of tumor makers in 10 min.[37] Taking advantage of the ultrahigh brightness of polymer dots, the detection limit was improved by 2 orders of magnitude compared to QD-based ICTSs.[37]

In this study, we have developed an ICTS-based sensor using polymer dots for enhanced sensitivity. Ultrastabilized and ultrabright polymer carbon dots (PCDs) were synthesized as labels for dual-channel ICTSs to detect cypermethrin (a representative pyrethroid insecticide) and 3-PBA. A smartphone-based device was developed for on-site sample analysis. The proposed platform features three improvements over conventional techniques: (1) PCDs with ultrahigh brightness instead of common QDs to improve the sensitivity and stability; (2) dual-channel ICTSs implemented for simultaneous detection of cypermethrin

and 3-PBA, providing more comprehensive biomonitoring exposure to cypermethrin; and (3) a smartphone-based device with software for direct analysis and recording of results for on-site evaluation of cypermethrin exposure.

EXPERIMENTAL SECTION

Materials and Reagents.

para-Aminosalicylic acid (PAS), ethanol, poly(D,L-lactide-*co*-glycolide)-COOH (PLGA-COOH) (lactide/glycolide, 1:1, mole/mole, molecular weight 20,000), polyvinyl alcohol (PVA), acetonitrile, hydrochloric acid, sodium chloride, dichloromethane (DCM), phosphate buffered saline (PBS, pH 7.4, 0.01 M), 3-PBA, cypermethrin analytical standard, sucrose, bovine serum albumin (BSA), Tween-20, Goat anti-mouse IgG antibody, and anti-HA-peroxidase were purchased from Sigma-Aldrich (St. Louis, MO). The 3-PBA-coating antigen and anti-3-PBA antibody (anti-3-PBA Ab, the antibody is the nanobody, VHH) were obtained from Dr. Hammock's group (University of California, Davis). The pyrethroid-coating antigen [BSA] [DAGF-203] (haptens used to prepare the pyrethroid-coating antigen are shown in Figure S1), mouse anti-pyrethroid monoclonal antibody (anti-pyrethroid Ab), and clone P-2 (CABT-L1975) (the cross-reactivity for cypermethrin was 100%) were purchased from Creative Diagnostics (Shirley, NY). Human urine samples were purchased from Bioreclamation IVT (Hicksville, NY). The nitrocellulose membrane, sample pad (glass fiber), conjugated pad (glass fiber), backing cards, and absorbent pad were purchased from Millipore (Billerica, MA). Ultrapure water obtained from a Millipore Milli-Q water purification system was used for experiments.

Apparatus.

Separation of the PCD-conjugated antibody was performed using centrifugation (Eppendorf 5417C; Eppendorf). The test strip was fabricated using a guillotine cutting system (Bio Dot Ltd). The pyrethroid-coating antigen and 3-PBA-coating antigen were dispensed on the nitrocellulose membrane using a BioDot BioJet BJQ 3000 dispenser (Irvine, CA). The fluorescence spectrum was measured using a Tecan Safire2 microplate reader (Tecan, Switzerland). The transmission electron microscopy (TEM) images were obtained with a Philips CM200UT instrument. A smartphone, iPhone SE (Apple Inc., CA), was used for signal capturing and processing. The smartphone-based device was printed on a 3D printer (Hangzhou Shining 3D Tech Co., China).

Synthesis of Carbon Dots.

Carbon dots were prepared by heating 0.2 g of PAS in ethanol (20 mL) at 200 °C for 18 h in a Teflon autoclave and purified using a tubular dialysis membrane.[38] After cooling down to room temperature, a dark solution was obtained. The dark solution was purified with a dialysis bag (MWCO ~ 1.0 kDa) and dialyzed against water for 1 day to remove small molecules, replacing the water every 6 h. Finally, carbon dots were freeze-dried to a black solid. The resulting carbon dots can uniformly disperse in aqueous matrices, resulting in a brown solution in the water matrix or a dark red solution in the PBS matrix.

Preparation of PCDs.

PCDs were prepared by a modified spontaneous emulsification solvent diffusion method according to previous studies with modification.[39] Briefly, 2 mg of PLGA-COOH was dissolved in 1.0 mL of acetonitrile which contains 0.2 mg of carbon dots. The PLGA/carbon dot solution was quickly added into 10 mL of phosphate buffer (1xPBS) containing 1% PVA under stirring. After incubation for 1 h, the PCDs were centrifuged and washed with PBS. The obtained PCDs were resuspended into 5 mL of PBS for further use.

Preparation of the PCD-Conjugated Antibody (PCDs-Ab).

Antibody-modified PCDs were prepared using a non-covalent immobilization technique which was widely used in preparation of gold nanoparticle-labeled antibodies.[40,41] At the pH slightly higher than the isoelectric point of antibody (protein), the positively charged amino groups can tightly bind to the negatively charged surface of PCDs. In detail, the pH of the PCD (1 mL, 0.1 mg/mL) solution was first adjusted to 8.2–8.5 by adding 0.02 M K_2CO_3. Then, 30 μL of anti-pyrethroid Ab (1 mg/mL) or anti-3-PBA Ab (0.6 μg/mL) was added into the adjusted PCD solution. After 60 min of gentle stirring at room temperature, 110 μL of 10.0 wt % BSA was added to the mixture followed by 30 min of incubation. Afterward, the mixture was centrifuged at 13,500 rpm for 7 min, and the red precipitate was washed twice with PBS (pH 7.4) containing 1% BSA. Finally, the resultant PCD-conjugated Ab (PCDs-pyrethroid Ab or PCDs-3-PBA Ab) was suspended in 150 μL of PBS (pH 7.4) containing 2% BSA and 3% sucrose and stored at 4 °C before use.

Preparation of Dual-Channel ICTSs.

The dual-channel ICTS was prepared according to our previous method (Figure 1A).[42] The sample pad and conjugated pad were first immersed in blocking buffer (PBS containing 1% BSA and 0.25% Tween-20). The pyrethroid-coating antigen (30 μL, 1 mg/mL) or 3-PBA-coating antigen (1 mg/mL) was dispersed on the test line. Similarly, 30 μL of the goat anti-mouse IgG antibody or anti-HA-peroxidase was dispersed on the control line. There was about a 1 cm distance between the two lines. Then, the sample pad, conjugated pads, and nitrocellulose membranes were dried overnight at RT. Then, each pad was immobilized on a PVC backing with 2 mm mutual overlap. Afterward, the ICTS was cut at a width of 4 mm, and two ICTSs (pyrethroid and 3-PBA channel) were attached onto a shared sample pad, as presented in Figure 2A. Finally, each PCDs-Ab conjugation was precoated on the corresponding conjugate pads using a pipette and dried at 37 °C.

Urine Matrix Standards.

Urine matrix samples were prepared using a modified method to hydrolyze phase II conjugates of 3-PBA for biomonitoring.[43] Urine samples (10 mL) were treated with 0.5 mL of HCl (37%) and 1 mL of DCM. Samples were sealed and heated at 80 °C for 60 min. NaCl (10%) was added after samples were cooled to room temperature, and samples were extracted using 10 mL of DCM. Using this method, 100 mL of the DCM extract was prepared and eventually extracted into 10 mL of methanol through solvent exchange. The resulted hydrolyzed methanol extract was 10-fold diluted and stored at 4 °C before use. The

as-prepared hydrolyzed urine extract was mixed with PBS containing 0.25% Tween-20 (1:5) when making the 3-PBA-spiked urine matrix standard.

Design of Smartphone-Based Devices.

The fluorescence spectrometer attachment for iPhone SE was designed in SolidWorks, which mechanically aligns a diffraction grating (GT13–12; Thorlabs Inc., NJ, USA), a long-pass filter (NT48–354; Edmund Optics Inc., NJ, USA), and a collimating lens (NT63–491; Edmund Optics Inc.). One commercial blue laser diode was used as the excitation light source to provide narrow-band excitation centered at 405 nm with an output of 5 mW. The fluorescence emission was collected and separated from the excitation and background via a long-pass filter positioned behind the sample. The fluorescence emission was focused along only one axis onto the transmission diffraction grating (1200 lines/mm) at a 47° angle with respect to the light path in order to satisfy the grating first-order diffraction mode. Magnified fluorescent spectrum images were formed and collected with both the external and built-in lens of the iPhone camera and then recorded using the CMOS sensor chip. The internal camera is sensitive to wavelengths within the visible spectrum, $400 < \lambda < 700$ nm. For spectrum analysis, the spectrum was determined by the smartphone application (Go Spectro).

Assay Procedure.

In a typical test, 70 μL of sample solution (PBS containing 0.25% Tween-20 with different concentrations of sample) was loaded onto the triangular-like sample pad and diffused through capillary force (Figure 1A). After a complete competitive immunoreaction between the coating antigen and sample solution, PCDs were quantitatively captured on the test lines and control line (Figure 1B). The red fluorescence appeared gradually in both test lines and the control line under the excitation light. The control line indicated that the ICTS worked well and the signal at the test line was reliable. Afterward, the ICTS was inserted into a plastic card (Figure 2C) and placed in the 3D-printed device (Figure 2D). The smartphone, smartphone holder, and the 3D-printed accessory were assembled into a complete detection device. The excitation light source was turned on, and the fluorescence intensity was recorded using the smartphone self-contained application (Go Spectro) (Figure 2E). The application can provide the fluorescence spectrum directly which simplified the data analysis. More details are presented in Figure S2.

RESULTS AND DISCUSSION

Structure of the 3D-Printed Device.

A fluorescent ICT analyzer was designed and fabricated, which can be easily integrated with a smartphone for rapid quantification of fluorescence intensity. The device comprises a 3D-printed cartridge, excitation light source, a set of lenses including an edge pass filter lens, and a diffraction grafting lens, as presented in Figures S2 and S3. As the excitation light source (405 nm, 5 mW) illuminates the PCDs, the emitted light passes through the edge pass filter lens (cut-on 500 nm), which filters short-wavelength background and noise. The transmission light then passes through a diffraction grating lens (1200 grooves/mm, 36.9° groove angle) at an orientation of 47° for maxima diffracted light intensity of first-order

diffraction, which is captured using the CMOS image sensor of the embedded camera of a smartphone. The fluorescence signal is processed in real time through an image processing application (Go Spectro).

Characteristics of PCDs.

The morphology of carbon dots was investigated by TEM. As revealed in Figure S4A, the as-prepared carbon dots were well-dispersed and exhibited a spherical shape with a diameter of approximate 6 nm with a homogeneous spherical structure. Figure S4B shows the high-resolution TEM (HRTEM) image of carbon dots, and it is clear that carbon dots have highly crystalline structures with well-resolved lattice fringes. The introduction of nitrogen groups may play an important role for the increase in interlayer distance. An interplanar distance of 0.21 nm was observed, representing the (001) plane of graphite. The graphitic feature is also confirmed by the observation of the D band at ~1350 cm^{-1} and the G band at ~1582 cm^{-1}, referring to different hybridization states of carbon structures, from the Raman spectrum, as presented in Figure S4C. As the integrated intensity ratio I_D/I_G of the two bands is widely used to determine the density of defects for graphitic materials, the calculated value (0.83) indicates a relatively high degree of crystallization, which agrees with the result of Figure S4B. To confirm the existence of nitrogen in the carbon dots synthesized, X-ray photoelectron spectroscopy (XPS) was applied. As presented in Figure S4D, three large peaks were observed, referring to the electron configurations of C 1s (74.3%), N 1s (8.5%), and O 1s (16.1%). The doped nitrogen could be the reason of the increased interlayer distance (0.40 nm, $2\theta = 22°$) calculated from the XRD spectrum (Figure S5). The wide diffraction peak also indicates an amorphous carbon phase. The C–N groups can enhance the room temperature phosphorescence, and the amide nitrogen atoms can increase the formation of hydrogen bonds, which were associated with the optical/fluorescence properties.[38]

The PCDs were prepared by a modified spontaneous emulsification solvent diffusion method. In detail, carbon dots were first mixed with PLGA-COOH solution (dissolved in acetonitrile) to form a homogeneous solution. This solution was then added into a PBS solution (prefiltered through a 0.22 nm filter) with stirring at 450 rpm using a laboratory magnetic stirrer. During preparation of the PCDs, the diffusion of the solvent played an important role in stabilizing the complex structure. The TEM images (Figure 3A) demonstrated that the PCDs were uniformly dispersed with an average particle size of 60 nm. Previous studies indicated that the encapsulating matrix could protect fluorescence from self-quenching by acting as a spacer to prevent the interaction of neighboring dye via energy transfer. The ultrahigh brightness of PCDs could be attributed to the cage effect, by which the carbon dots encapsulated in nanospheres are confined by the network, and this suppressed nonradiation decay of the photoexcited state. To test whether PCDs could be prospective labels for biological assay, the stability of PCDs needed to be further investigated. The photoluminescence stability of PCDs to long-term UV exposure, storage time, and pH conditions was investigated. PCDs exhibited high chemical and colloidal stability for long-term storage (30 days) in solution, which is significant for preservation and transportation (Figure 3B). However, under the same condition, the emission intensity of carbon dots drastically decreased to 33% after 30 days of storage. Upon UV exposure,

photoluminescence intensities of both PCDs and carbon dots continuously decreased, while photoluminescence decay of carbon dots was much faster than that of the sample of PCDs. After 8 h, obvious photobleaching was found for carbon dot samples, whose photoluminescence intensity was reduced to 48%, while the PCD sample maintained a higher value of up to 81% (Figure 3C). The corresponding peak positions of the PCDs showed a negligible change, suggesting that it had better anti-photobleaching properties than the carbon dots. Another interesting phenomenon is pH-induced photoluminescence properties. The photoluminescence intensity of carbon dots decreased at high or low pH, whereas it remained steady in the pH range from 6 to 10. However, the photoluminescence intensities of PCDs are well maintained across a broad pH range (4–12) (Figure 3D). Even at a low pH value of 3, the PCDs still maintained 48% emission intensity. The abovementioned results indicate that the PLGA nanoparticles effectively protect the surface state or molecular state of carbon dots apart from the influence of the solvent environment.

The PCD-antibody conjugations were formed through electrostatic adsorption between the negatively charged surface of PCDs and the positively charged amino groups. To demonstrate this process, the zeta potentials of the PCDs before and after conjugating with antibodies were tested. As shown in Figure S6, the zeta potential of the PCDs was approximately −43.4 mV. After conjugation with anti-pyrethroid Ab or anti-3-PBA Ab, the zeta potential was −22.8 and −30.3 mV, respectively. The distinctive change in the zeta potential indicated the successful conjugation procedure.

In general, the fluorescence intensity of labels decreases after conjugation to proteins. Therefore, whether conjugation of the PCDs could retain their fluorescence intensity was investigated. As shown in Figure 4, the inset shows the digital photograph of PCDs and modified PCDs (conjugated to anti-3-PBA Ab and anti-PY Ab) under 365 nm UV light. To the naked eye, the fluorescence intensities of the three tubes are almost identical, which reveals that fluorescence was largely unchanged after modification. This conclusion was supported by the fluorescence spectrum. The abovementioned results demonstrated that the Ab-modified PCD conjugation had similar fluorescence intensity to the PCDs.

Principle of Proposed Assay.

In order to better monitor the exposure of pyrethroids, simultaneous detection of cypermethrin and its metabolite (3-PBA) was used. In view of the nonspecific adsorption and the limitation of Washburn's theory,[44,45] two test strips were assembled in parallel instead of applying the two test lines on one single test strip (Figure 1A). The limitation of simply adding two test lines in a single test strip is that it may generate unexpected cross-reaction, enlarged assay time, and erratic nanomaterial distribution.[45,46] The proposed dual-channel ICTS exhibited the same detection performance as great as each single channel set. In addition, PCDs, instead of common QDs, as the signal amplifier further improved the stability and sensitivity of the dual-channel ICTS (Figure 1B). This is because of the effect of the polymer cage, by which the carbon dots encapsulated in nanospheres are confined and the network suppresses non-radiation decay of the photoexcited state. Thus, the nanosphere not only integrated the total fluorescence of all embedded carbon dots but also effectively protected the surface state or molecular state of carbon dots apart from the influence of

the solvent environment, which made the PCDs become stable and ultrabright. Finally, to make the method more suitable for on-site applications, the smartphone-based device integrated with a light source, an optical grating, a 3D-printed holder, and a smartphone with self-contained analysis software was developed to record the results (Figure 2). To sum up, the proposed ICTS assay is hand-held and sensitive without any sophisticated sample pretreatment and laboratory-based instruments, making it a widely applicable tool for the analysis of exposure to pyrethroids.

Specificity.

Since 3-PBA has a similar chemical structure to many pyrethroids (cypermethrin, permethrin, deltamethrin, etc.), cross-reactivity can occur between the parent compound antibody and the metabolite antigen or vice versa. However, the specificity of the antibody is an extremely critical factor for dual-channel ICTSs. Therefore, the cross-reactivity of the proposed ICTS assay was tested. As shown in Figure 5A, PCDs-pyrethroid Ab was used in recognition of the coating antigen of pyrethroids (a) and the coating antigen of 3-PBA (b). As measured using the smartphone-based device, the fluorescence intensity of curve (a) is significantly stronger than that of curve (b). The fluorescence intensity of curve (b) was close to the blank test strip signal (see the background), indicating that the cross-reaction could be ignored. We also explored the cross-reactivity between anti-3-PBA Ab and the coating antigen of pyrethroid (Figure 5B). Similarly, a weak fluorescent intensity was observed on curve (d) compared to the intensity of curve (c), indicating that the cross-reactivity was negligible. The abovementioned results revealed that both antibodies have excellent specificity, which is consistent with data provided by the antibody producers.[47] In addition, the single-domain antibody, that is, nanobody, was used for 3-PBA detection in this work rather than conventional antibodies. Nanobodies have been an attractive alternative to conventional antibodies due to their superior solubility, stability, and economy, which also possess smaller size and specificity/affinity as good as conventional antibodies.[13]

Optimization of Experimental Conditions.

Conditions such as the amount of PCDs-pyrethroid Ab, amount of PCDs-3-PBA Ab, and immunoreaction time were optimized for obtaining the best analytical performance of the experimental system. Here, the ratio of the signal (fluorescence intensity recorded in the absence and presence of cypermethrin or 3-PBA in the sample) was selected as the criteria. The target (cypermethrin or 3-PBA) concentration used was 1 ng/mL. As the coating antigen on the test line for the pyrethroid is constant, the amount of the PCDs-pyrethroid Ab preloaded on the conjugation pad was of vital importance. As displayed in Figure S7A, the highest ratio of the signal was obtained with 2 μL of PCDs-pyrethroid Ab on the conjugation pad, indicating that it is the optimal amount for the competitive immunoreaction. Similarity, 3 μL of PCDs-pyrethroid Ab on the conjugation pad was the optimal amount to achieve the best competitive effect (Figure S7C).

The ratio of the signal in different assay times for the two immunoreactions was tested to obtain the optimal incubation time. Several immunoreaction times including 2, 5, 7, 10, 15, and 20 min were chosen for this study. The maximum ratios were achieved at 10 min for cypermethrin (Figure S7B) and 7 min for 3-PBA (Figure S7D), indicating that the

immunoreaction attained saturation at these times. Therefore, according to the experimental results, the optimal conditions for the detection of cypermethrin and 3-PBA can be described as follows: the amount of PCDs-pyrethroid Ab was 2 μL, the amount of PCDs-3-PBA Ab was 3 μL, the immunoreaction time for cypermethrin was 10 min, and the immunoreaction time for 3-PBA was 7 min.

Urine Matrix Effect.

3-PBA, as a typical biomarker of exposure to pyrethroid (e.g., cypermethrin) pesticides, is generally measured in urine samples. Thus, we evaluated the ability of the sensor to detect 3-PBA in an acid-treated urine matrix[43] to validate its feasibility in real urine sample analysis. For immunoassay-based measurement of 3-PBA in urine, an additional acid hydrolysis process is generally used to release 3-PBA from its phase II conjugated forms. A comparison between the PBS standard solution and the hydrolyzed urine matrix was conducted for 1, 10, and 50 ng/mL 3-PBA (Figure 6). The hydrolyzed urine matrix (spike urine standard) was prepared as described in Experimental Section, of which no statistic matrix effect was observed compared to results of the PBS matrix in ELISA. The elimination of urinary matrix influence is due to two reasons: (1) the sample clean-up procedures through liquid-phase extraction reduced interferences and (2) the dilution of the urine extract by PBS assay buffer resulted in removal of matrix effects. Results demonstrate the feasibility of the proposed strategy to detect 3-PBA in an acid-treated urine matrix, such as those commonly used in biomonitoring studies.[43]

Performance of Dual-Channel ICTSs.

Under optimal conditions, the performance of the dual-channel ICTS was examined with the desired concentration of cypermethrin and the 3-PBA standard sample. Figure S8 displays the typical photographs of the dual-channel ICTS with different concentrations of cypermethrin (0, 1, 5, 10, 20, 50, and 100 ng/mL) and 3-PBA (0, 0.1, 1, 5, 10, 50, and 100 ng/mL). The red fluorescence in the test line decreases with the increase in target concentration since the competitive immunoreaction was adopted in the proposed dual-channel ICTSs. Quantitative detection was implemented by recording the peak intensity of the test lines. As seen in Figure 7, the peak intensity for detecting cypermethrin (A and C) and 3-PBA (B and D) decreased logarithmically with increasing concentration of the analyte from 1 to 100 and 0.1 to 100 ng/mL, respectively. The regression equations were $y = -10.340 \ln(x) + 66.747$ ($R^2 = 0.980$) for cypermethrin and $y = -11.860 \ln(x) + 75.307$ ($R^2 = 0.983$) for 3-PBA. The limits of detection (3S/N) were calculated to be ~0.35 ng/mL for cypermethrin and 0.04 ng/mL for 3-PBA, demonstrating a high sensitivity for simultaneous detection of cypermethrin and 3-PBA, which is contributed by the ultrahigh brightness of PCDs for signal enhancement and the parallel design of dual detection for noninterference. Furthermore, the RSD assays were performed for evaluating the stability for the detection of the two targets at low (1 ng/mL), medium (10 ng/mL), and high (50 ng/mL) concentrations. The RSD values were 6.4, 4.2, and 8.3%, respectively, indicating acceptable reproducibility of the dual-channel ICTS assay.

CONCLUSIONS

In summary, this work reported a technology for simultaneous detection of individual pyrethroids and their metabolite, 3-PBA, which provides a comprehensive and accurate biomonitoring method for exposure to pyrethroids. The novelty of this approach relies on the facts that (1) PCDs were synthesized with ultrahigh brightness and applied as the fluorescence signal reporter, and due to the cage effect, the carbon dots encapsulated in nanospheres are confined by the polymer network that effectively protected the surface state or molecular state of carbon dots apart from the influence of the solvent environment, improving the stability and sensitivity of the dual-channel ICTS, and (2) the universal smartphone and its self-contained application were utilized to record results directly without any complex data processing, making this method attractive for rapid screening of potential pyrethroids exposure in field and point-of-care diagnostics. Thus, the dual-channel ICTS assay has advantages including dual-channel assay, low cost, high sensitivity, and simple operation, making it suitable for on-site applications in a wide range of environments.

Supplementary Material

Refer to Web version on PubMed Central for supplementary material.

ACKNOWLEDGMENTS

This work was supported by the Centers for Disease Control and Prevention/National Institute for Occupational Safety and Health (CDC/NIOSH) grant no. R01OH011023-01A1. We acknowledge the financial support for antibody development from The National Institute of Environmental Health Science Superfund Research Program (P42ES004699) and the National Institute of Environmental Health Sciences RIVER Award (NIEHS, R35 ES030443-01). The opinions, findings, conclusions, or recommendations expressed in this paper are those of the authors alone and do not necessarily reflect the views of NIH and CDC.

REFERENCES

(1). Pérez JJ; Williams MK; Weerasekera G; Smith K; Whyatt RM; Needham LL; Barr DBJ Chromatogr. B: Anal. Technol. Biomed. Life Sci 2010, 878, 2554–2562.

(2). Amweg EL; Weston DP; Ureda NM Environ. Toxicol. Chem 2005, 24, 966–972. [PubMed: 15839572]

(3). Shafer TJ; Meyer DA; Crofton KM Health Perspect. 2005, 113, 123–136.

(4). Ahn KC; Kim H-J; McCoy MR; Gee SJ; Hammock BD J. Agric. Food Chem 2011, 59, 2792–2802. [PubMed: 21105656]

(5). Ahn KC; Gee SJ; Kim H-J; Aronov PA; Vega RI; Hammock BD; Hammock BD Anal. Bioanal. Chem 2011, 401, 1285–1293. [PubMed: 21717113]

(6). Shan G; Huang H; Stoutamire DW; Gee SJ; Leng G; Hammock BD Chem. Res. Toxicol 2004, 17, 218–225. [PubMed: 14967009]

(7). Han Y; Xia Y; Han J; Zhou J; Wang S; Zhu P; Zhao R; Jin N; Song L; Wang X Chemosphere 2008, 72, 785–790. [PubMed: 18479728]

(8). Aylward LL; Irwin K; St-Amand A; Nong A; Hays SM Regul. Toxicol. Pharmacol 2018, 92, 29–38. [PubMed: 29113940]

(9). Personne S; Marcelo P; Pilard S; Baltora-Rosset S; Corona A; Robidel F; Lecomte A; Brochot C; Bach V; Zeman F Anal. Bioanal. Chem 2019, 411, 8043–8052. [PubMed: 31748895]

(10). Jeong D; Kang JS; Kim KM; Baek S-H; Choe S; Pyo J Forensic Sci. Int 2019, 302, 109846. [PubMed: 31255840]

(11). Schettgen T; Dewes P; Kraus T Anal. Bioanal. Chem 2016, 408, 5467–5478. [PubMed: 27240420]

(12). Kavvalakis MP; Tzatzarakis MN; Alegakis AK; Vynias D; Tsakalof AK; Tsatsakis AM Drug Test. Anal 2014, 6, 9–16. [PubMed: 24817043]

(13). Huo J; Li Z; Wan D; Li D; Qi M; Barnych B; Vasylieva N; Zhang J; Hammock BD J. Agric. Food Chem 2018, 66, 11284–11290. [PubMed: 30293433]

(14). Ahn KC; Lohstroh P; Gee SJ; Gee NA; Lasley B; Hammock BD Anal. Chem 2007, 79, 8883–8890. [PubMed: 17983205]

(15). Wengatz I; Stoutamire DW; Gee SJ; Hammock BD J. Agric. Food Chem 1998, 46, 2211–2221.

(16). Shan G; Stoutamire DW; Wengatz I; Gee SJ; Hammock BD J. Agric. Food Chem 1999, 47, 2145–2155. [PubMed: 10552511]

(17). Shan G; Leeman WR; Stoutamire DW; Gee SJ; Chang DPY; Hammock BD J. Agric. Food Chem 2000, 48, 4032–4040. [PubMed: 10995309]

(18). Matveeva EG; Shan G; Kennedy IM; Gee SJ; Stoutamire DW; Hammock BD Anal. Chim. Acta 2001, 444, 103–117.

(19). Lee H-J; Shan G; Watanabe T; Stoutamire DW; Gee SJ; Hammock BD J. Agric. Food Chem 2002, 50, 5526–5532. [PubMed: 12236674]

(20). Ahn KC; Watanabe T; Gee SJ; Hammock BD J. Agric. Food Chem 2004, 52, 4583–4594. [PubMed: 15264887]

(21). Nichkova M; Dosev D; Gee SJ; Hammock BD; Kennedy IM Anal. Chem 2005, 77, 6864–6873. [PubMed: 16255584]

(22). Nichkova M; Dosev D; Davies AE; Gee SJ; Kennedy IM; Hammock BD Anal. Lett 2007, 40, 1423–1433. [PubMed: 19079795]

(23). Kim H-J; Ahn KC; Ma SJ; Gee SJ; Hammock BD J. Agric. Food Chem 2007, 55, 3750–3757. [PubMed: 17455946]

(24). Ouyang H; Lu Q; Wang W; Song Y; Tu X; Zhu C; Smith JN; Du D; Fu Z; Lin Y Anal. Chem 2018, 90, 5147–5152. [PubMed: 29590527]

(25). Cheng N; Shi Q; Zhu C; Li S; Lin Y; Du D Biosens. Bioelectron 2019, 142, 111498. [PubMed: 31319328]

(26). Cheng N; Song Y; Fu Q; Du D; Luo Y; Wang Y; Xu W; Lin Y Biosens. Bioelectron 2018, 117, 75–83. [PubMed: 29886189]

(27). Ouyang H; Tu X; Fu Z; Wang W; Fu S; Zhu C; Du D; Lin Y Biosens. Bioelectron 2018, 106, 43–49. [PubMed: 29414087]

(28). Ruan X; Wang Y; Kwon EY; Wang L; Cheng N; Niu X; Ding S; Van Wie BJ; Lin Y; Du D Biosens. Bioelectron 2021, 184, 113238. [PubMed: 33878594]

(29). Zhao Y; Yang M; Fu Q; Ouyang H; Wen W; Song Y; Zhu C; Lin Y; Du D Anal. Chem 2018, 90, 7391–7398. [PubMed: 29792679]

(30). Duan Z; Yin M; Zhang C; Song G; Zhao S; Yang F; Feng L; Fan C; Zhu S; Wang H Analyst 2018, 143, 392–395. [PubMed: 29239409]

(31). Duan Z; Zhang C; Qiao Y; Liu F; Wang D; Wu M; Wang K; Lv X; Kong X; Wang H Talanta 2017, 170, 306–313. [PubMed: 28501174]

(32). Seremba E; Ocama P; Opio CK; Kagimu M; Yuan HJ; Attar N; Thomas DL; Lee WM J. Med. Virol 2010, 82, 1334–1340. [PubMed: 20572076]

(33). Manta P; Agarwal S; Singh G; Bhamrah SS World J. Pharm. Pharmaceut. Sci 2015, 4, 1870–1905.

(34). Wang Q; Long M; Lv C; Xin S; Han X; Jiang W Food Contr. 2020, 109, 106894.

(35). Cai Y; Feng L; Hua Y; Liu H; Yin M; Lv X; Li S; Wang H Chem. Commun 2018, 54, 13595–13598.

(36). Zou Z; Du D; Wang J; Smith JN; Timchalk C; Li Y; Lin Y Anal. Chem 2010, 82, 5125–5133. [PubMed: 20507134]

(37). Fang C-C; Chou C-C; Yang Y-Q; Wei-Kai T; Wang Y-T; Chan Y-H Anal. Chem 2018, 90, 2134–2140. [PubMed: 29286241]

(38). Song Y; Zhu C; Song J; Li H; Du D; Lin Y ACS Appl. Mater. Interfaces 2017, 9, 7399–7405. [PubMed: 28134510]

(39). Lee S-J; Jeong J-R; Shin S-C; Kim J-C; Chang Y-H; Lee K-H; Kim J-D Colloids Surf., A 2005, 255, 19–25.

(40). Shemetov AA; Nabiev I; Sukhanova A ACS Nano 2012, 6, 4585–4602. [PubMed: 22621430]

(41). Jazayeri MH; Amani H; Pourfatollah AA; Pazoki-Toroudi H; Sedighimoghaddam B Sens. Bio-Sens. Res 2016, 9, 17–22.

(42). Cheng N; Song Y; Zeinhom MMA; Chang Y-C; Sheng L; Li H; Du D; Li L; Zhu M-J; Luo Y; Xu W; Lin Y ACS Appl. Mater. Interfaces 2017, 9, 40671–40680. [PubMed: 28914522]

(43). Chuang JC; Van Emon JM; Trejo RM; Durnford J Talanta 2011, 83, 1317–1323. [PubMed: 21238715]

(44). Cheng N; Shang Y; Xu Y; Zhang L; Luo Y; Huang K; Xu W Biosens. Bioelectron 2017, 91, 408–416. [PubMed: 28064126]

(45). Li J; Macdonald J Biosens. Bioelectron 2016, 83, 177–192. [PubMed: 27125840]

(46). Fenton EM; Mascarenas MR; López GP; Sibbett SS ACS Appl. Mater. Interfaces 2008, 1, 124–129.

(47). Kim H-J; McCoy MR; Majkova Z; Dechant JE; Gee SJ; Tabares-da Rosa S; González-Sapienza GG; Hammock BD Anal. Chem 2012, 84, 1165–1171. [PubMed: 22148739]

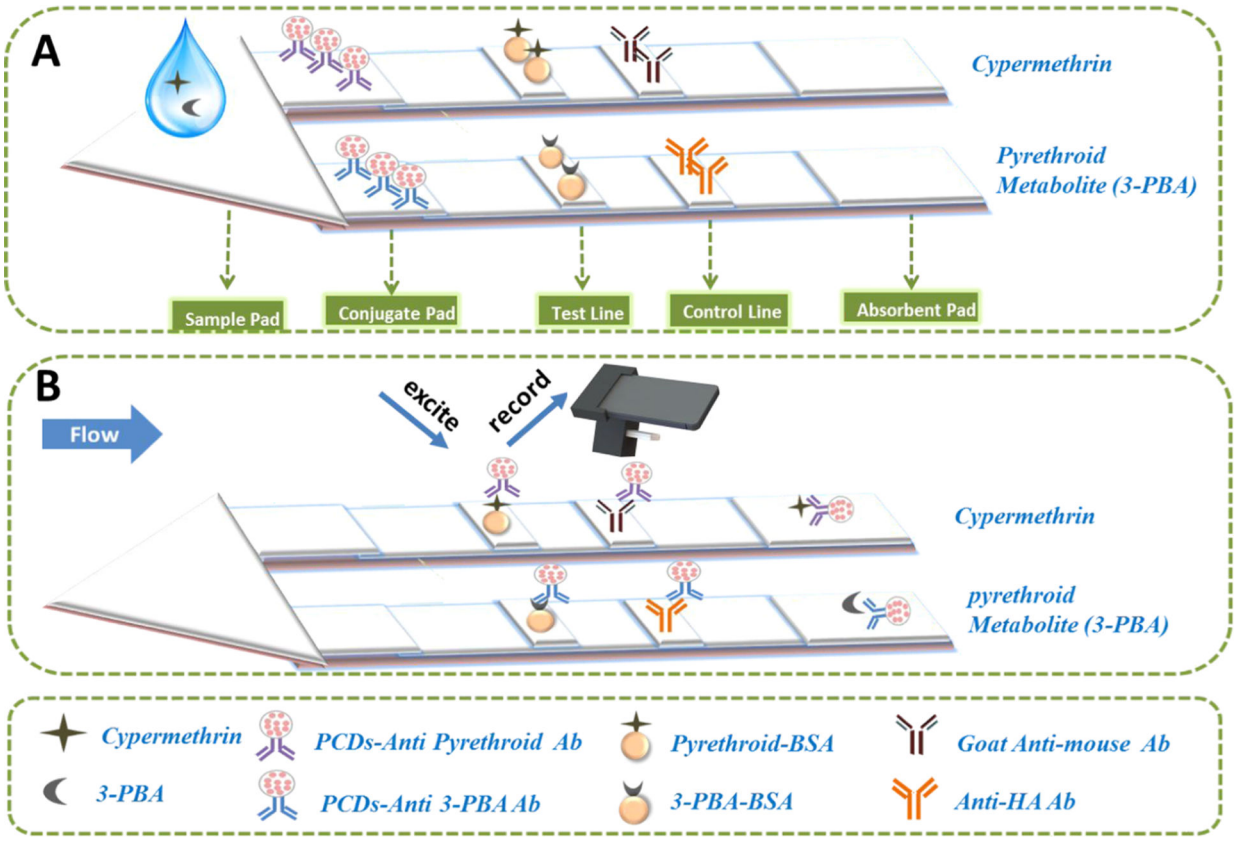

Figure 1.

(A) Scheme of dual-channel ICTSs for simultaneous detection of cypermethrin (model compound of pyrethroid) and 3-PBA and (B) using PCDs as probes to amplify the signal with a smartphone-based device as the signal reader.

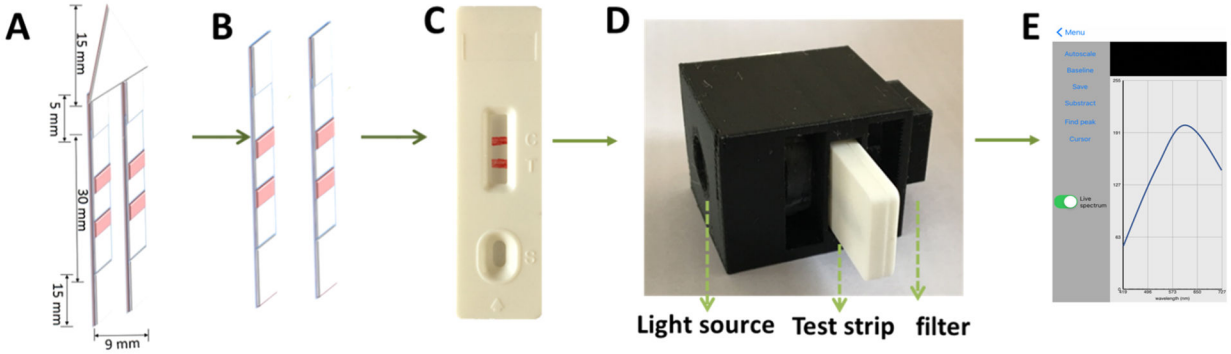

Figure 2.

(A–B) Dimensions of each part of dual-channel ICTSs, (C) plastic card integrated with test strips, (D) 3D-printed accessory, and (E) result of the fluorescence intensity on the final device.

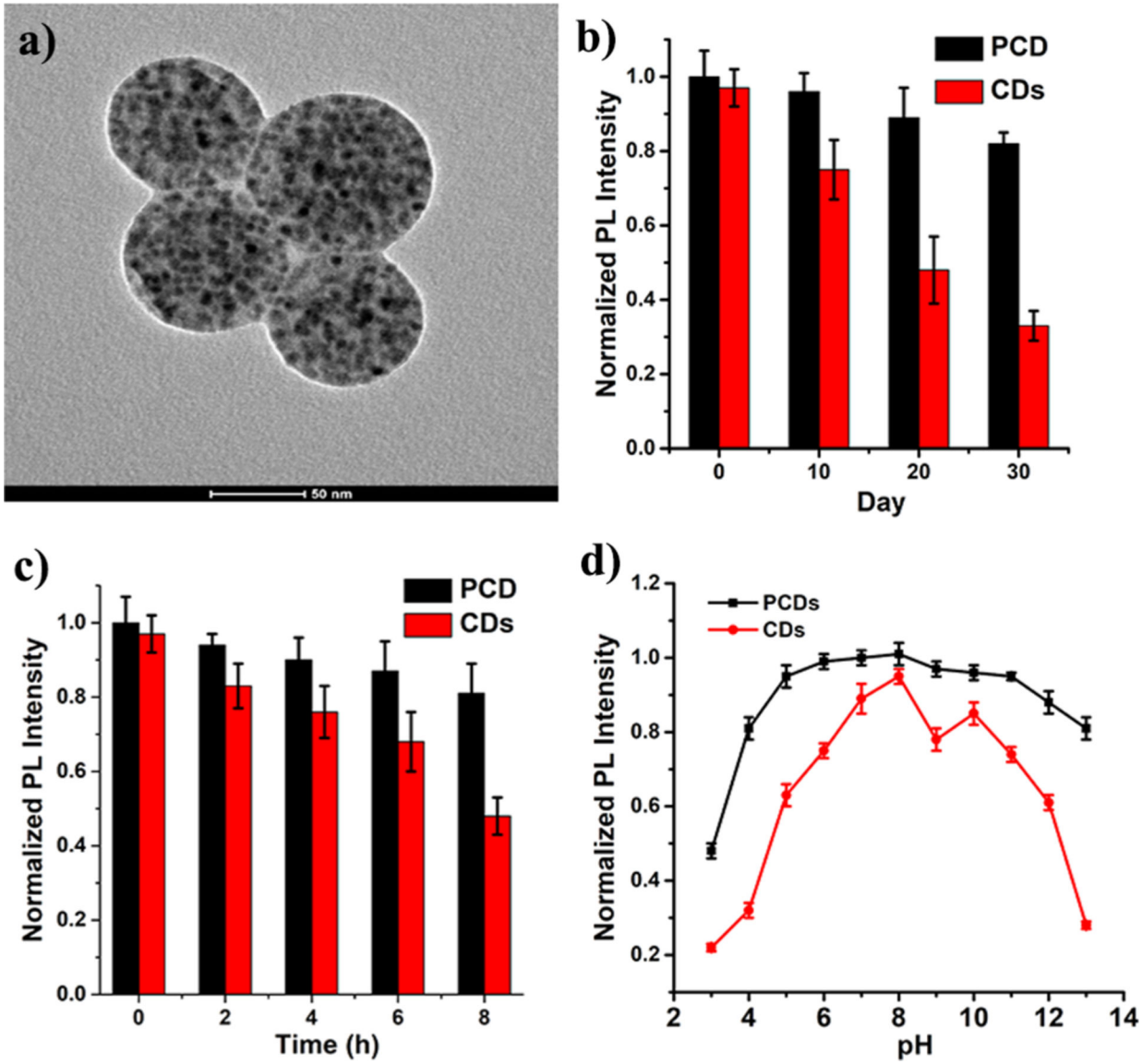

Figure 3.

(A) TEM image of PCDs, (B) fluorescence intensity of PCDs and carbon dots after long-term storage, (C) dependence of fluorescence intensity on the UV excitation time for PCDs and carbon dots in DI water, and (D) effect of pH on fluorescence intensity of PCDs and carbon dots.

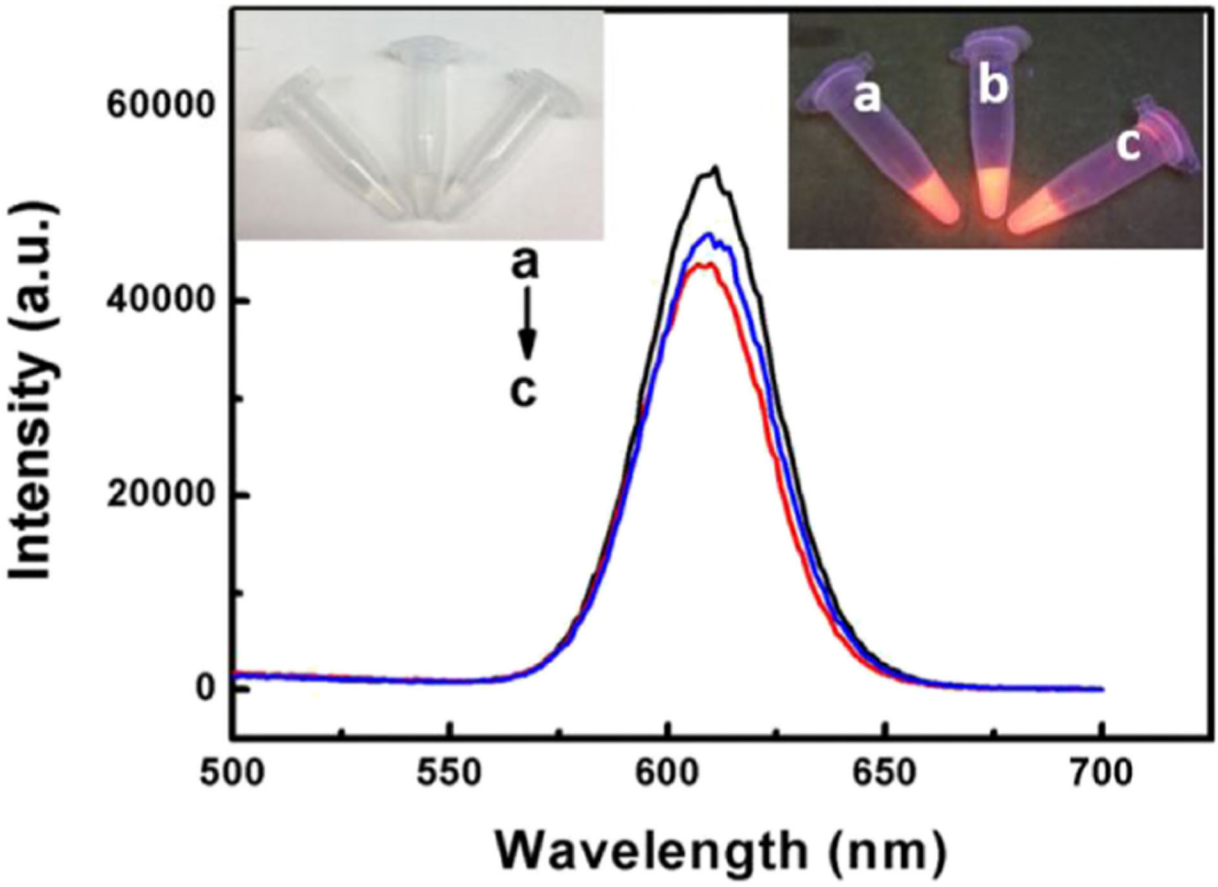

Figure 4.

Characteristics of PCD-conjugated Ab: 0.1 mg/mL PCDs (a), 0.1 mg/mL PCDs-pyrethroid Ab (b), and 0.1 mg/mL PCDs-3-PBA Ab (c). The fluorescence spectrum was recorded using a fluorescence spectrometer. The inset shows the digital photograph of PCDs and modified PCDs under sunlight (left) and 365 nm UV light (right).

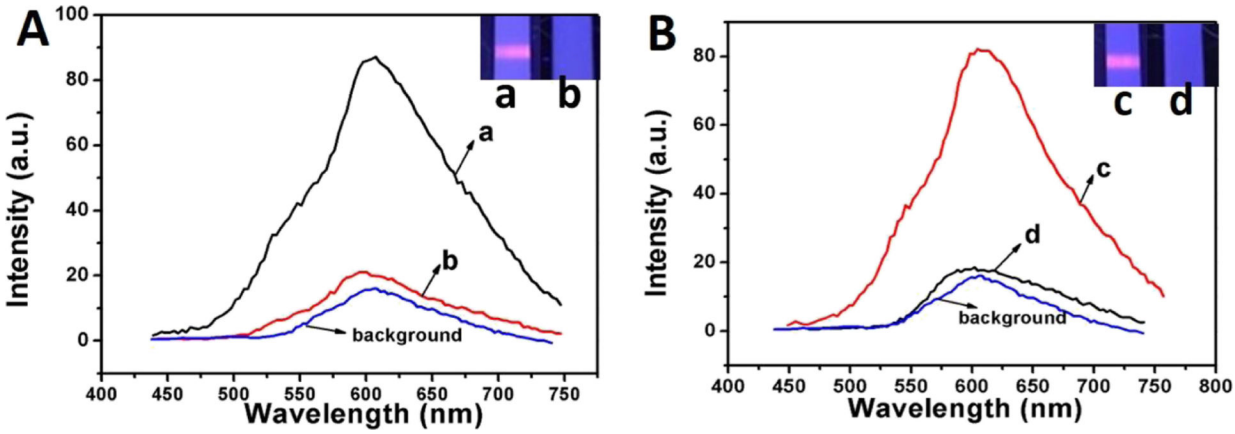

Figure 5.

Cross-reactivity: (A) using 2 μL of PCDs-pyrethroid Ab to recognize pyrethroid-BSA (a) and 3-PBA-BSA (b) and (B) using 2 μL of PCDs-3-PBA Ab to recognize 3-PBA-BSA (c) and pyrethroid-BSA (d). The fluorescence spectrum was recorded using our smartphone-based device.

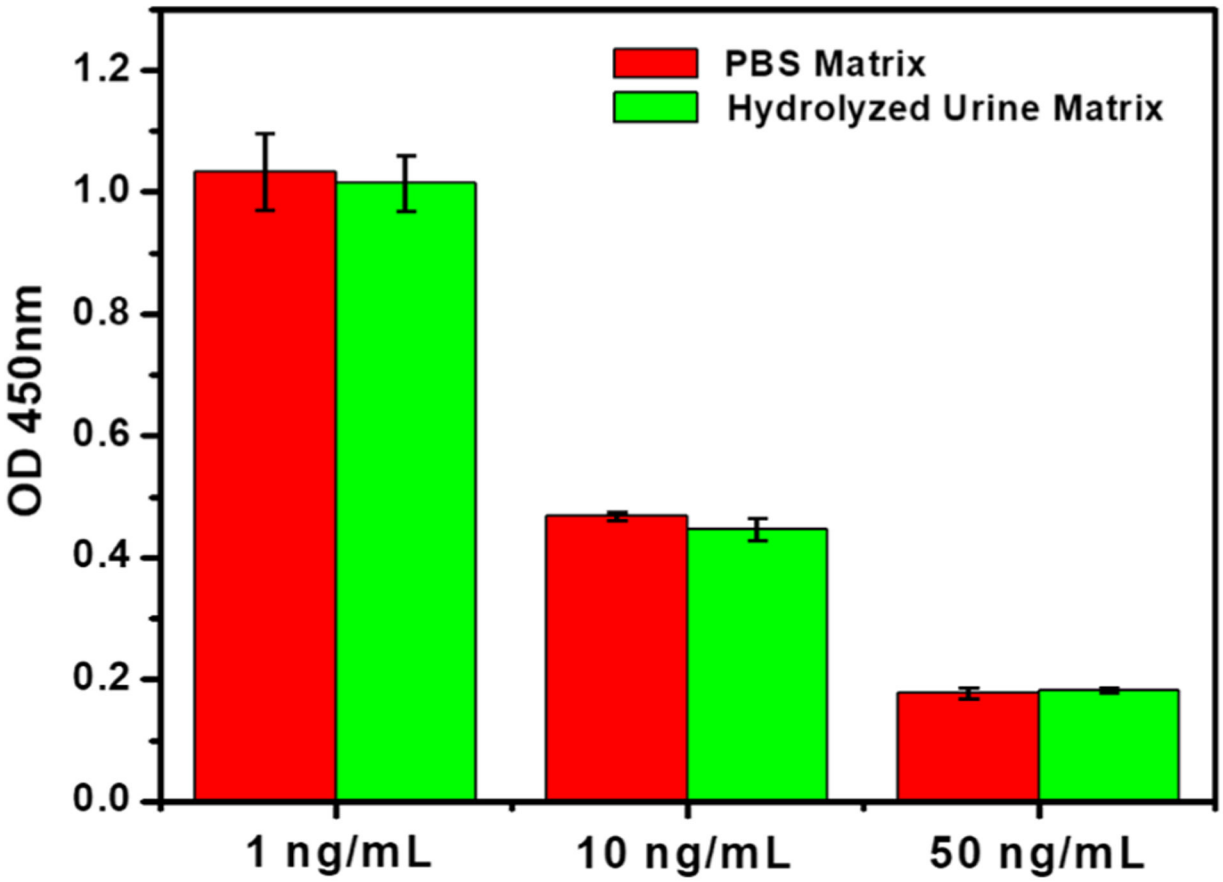

Figure 6.
Matrix effect of hydrolyzed urine compared to PBS standard solution at different concentrations of 3-PBA. No statistical difference was observed from OD results of ELISA.

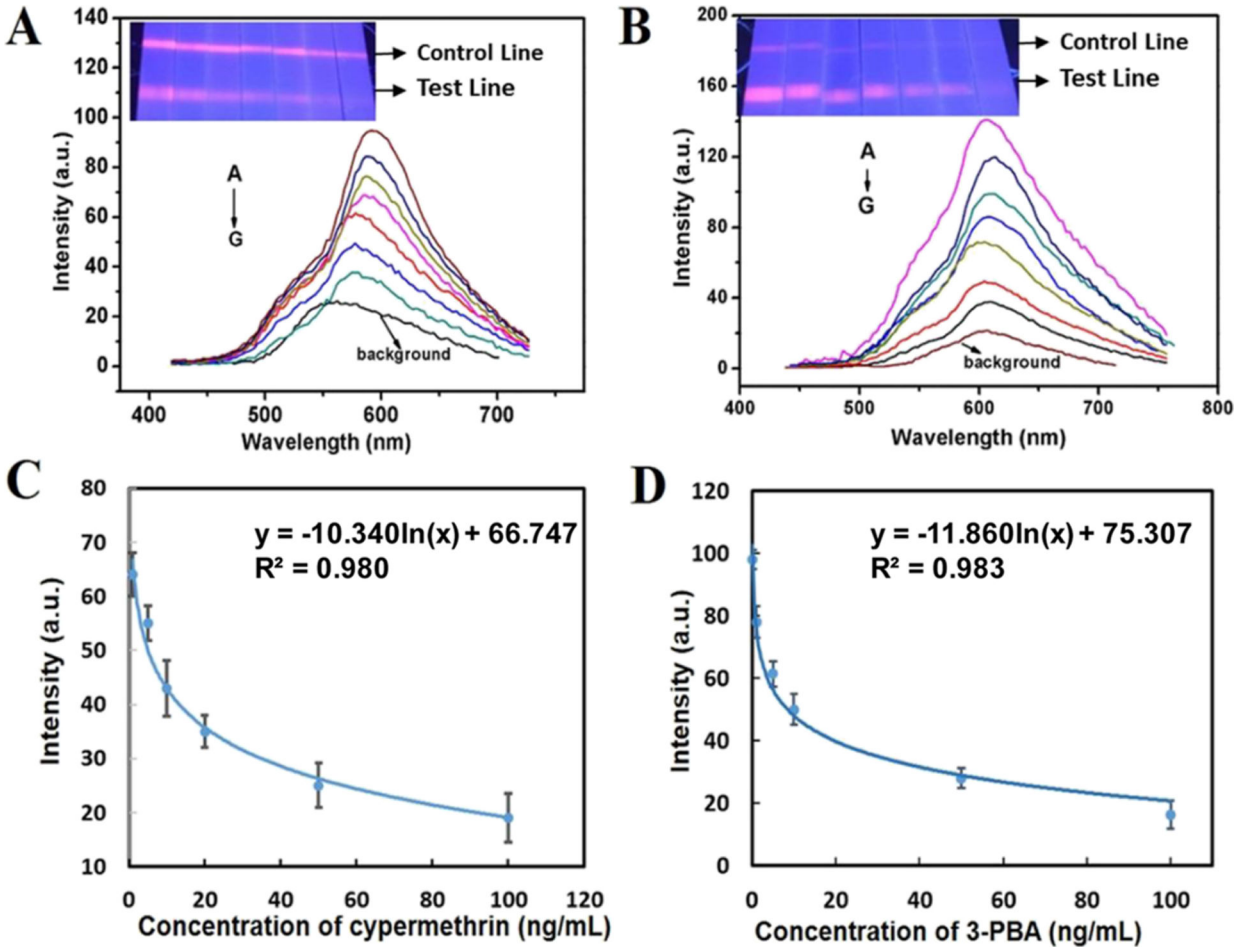

Figure 7.

Fluorescence intensity of the dual-channel ICTS (test lines) at different concentrations of cypermethrin (A) and 3-PBA (B) and calibration curves of fluorescence intensity vs target concentrations (C,D). Error bars indicate standard deviations of the three measurements.